Photoacoustics 43 (2025) 100716

Contents lists available at ScienceDirect

Photoacoustics

journal homepage: www.elsevier.com/locate/pacs

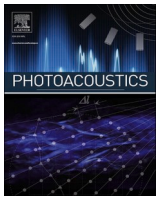

A clinical feasibility study of a photoacoustic finder for sentinel lymph node biopsy in breast cancer patients: A prospective cross-sectional study

Moongyu Han [a,1], Young Joo Lee [b,1], Junho Ahn [a], Sunghun Nam [a], Minseong Kim [a], Jeongwoo Park [c], Joongho Ahn [a], Hanyoung Ryu [d], Youngseok Seo [d], Byullee Park [e,*], Dooreh Kim [b,*], Chulhong Kim [a,*]

[a] Department of Convergence IT Engineering, Electrical Engineering, Mechanical Engineering, and Medical Science and Engineering, Medical Device Innovation Center, Pohang University of Science and Technology, 77 Cheongam-ro, Nam-Gu, Pohang 37673, Republic of Korea
[b] Department of Surgery, Seoul St. Mary's Hospital, College of Medicine, the Catholic University of Korea, 222 Banpo-daero, Seocho-gu, Seoul 06591, Republic of Korea
[c] Department of Biomedical Convergence Science and Technology, Kyungpook National University, Daegu 41566, Republic of Korea
[d] R&D Center, WONTECH Co. Ltd., Techno 8-ro, Yuseong-gu, Daejeon 34028, Republic of Korea
[e] Departments of Biophysics, Institute of Quantum Biophysics, Metabiohealth, Biopharmaceutical Convergence, Sungkyunkwan University, Suwon 16419, Republic of Korea

ARTICLE INFO

Keywords:
Non-radioactive sentinel lymph node detection
Sentinel lymph node biopsy
Photoacoustic
Photoacoustic finder

ABSTRACT

The sentinel lymph node (SLNb) is generally performed using radioisotopes, blue dyes, or both to improve false negative rate. However, ionizing radiation is involved in a gamma probe with radioisotopes and the blue dye detection relies on native visual inspection by an operator. To overcome these limitations, we developed the photoacoustic finder (PAF), a highly sensitive, non-radioactive detector that uses only blue dye and a photoacoustic signal to detect SLNs. A total of 121 patients with breast cancer were enrolled, and 375 lymph nodes were excised using conventional SLNb. The PAF was used to measure the signal from the excised lymph nodes. We compared the SLN detection rates of each method (gamma probe, visual inspection, and PAF) and conducted a non-inferiority test. The PAF detected 87 % of SLNs, comparable to the gamma probe (85 %) and superior to visual inspection (73 %). Non-inferiority tests confirmed PAF's performance was not inferior to visual inspection ($p < 0.001$) or the gamma probe ($p < 0.015$). Using the dual-modal method (gamma probe + visual inspection) as the gold standard, PAF showed a sensitivity of 0.81 and specificity of 0.63. This study demonstrates that PAF, using only blue dye, offers a non-inferior alternative to the standard dual-modal SLN detection method with radioactive materials, opening new avenues for radiation-free SLNb in the future.

1. Introduction

The presence of lymphatic metastases in breast cancer patients is an important prognostic factor for survival, and accurate staging leads to appropriate adjuvant treatment [1,2]. Sentinel lymph node biopsy (SLNb) is a standard method used to confirm regional axillary lymphatic metastases in breast cancer patients. Sentinel lymph nodes (SLNs) are a group of initial lymph nodes (LNs) located in proximity to the tumor and connected via lymphatic vessels (LVs), hypothetically the first ones that a primary tumor drains in the regional lymphatic basin. If metastatic tumor cells are not confirmed in the excised SLNs, the incidence of morbidities, such as lymphedema, can be reduced by omitting unnecessary axillary lymph node dissection (ALND) [3]. The SLNb procedure is a dual-modal method utilizing a radioactive tracer (e.g., $^{99\,m}$Tc) and/or blue dye to identify the SLNs [4,5]. The radioactive tracer and blue dye are administered before surgery and absorbed by the lymphatic system, and eventually they flow into the SLNs. During the surgical procedures, the SLNs are identified through visual inspection of blue-dyed LVs and radioactivity detection using a gamma probe. The identified SLNs are subsequently excised and sent for pathological

* Corresponding authors.
E-mail addresses: dalgyu0820@postech.ac.kr (M. Han), nofearyjbr@gmail.com (Y.J. Lee), jhahn60@postech.ac.kr (J. Ahn), shnam180260@postech.ac.kr (S. Nam), tjdgus3822@postech.ac.kr (M. Kim), jwpark@knu.ac.kr (J. Park), joongho.ahn@postech.ac.kr (J. Ahn), hyryu@wtlaser.com (H. Ryu), physys@wtlaser.com (Y. Seo), byullee@skku.edu (B. Park), rlaenfpd@gmail.com (D. Kim), chulhong@postech.edu (C. Kim).
[1] These authors contributed equally to this work.

https://doi.org/10.1016/j.pacs.2025.100716
Received 20 January 2025; Received in revised form 10 March 2025; Accepted 21 March 2025
Available online 28 March 2025

examination to assess the potential metastatic tumor.

The dual-modal method enhances the accuracy and efficiency of SLN identification by leveraging the distinct advantages of each method. However, the radioactive isotopes in the SLNb surgery present an inherent radiation exposure risk and necessitate specialized facilities and skilled medical personnel. These factors introduce complexities into the surgical procedure and create obstacles for the implementation of SLNb in local hospitals [6]. Moreover, the administration of radioactive material typically requires cooperation with a nuclear medicine department, which restricts direct usage by the surgeon and may impact surgical scheduling. Lastly, because radioactive isotopes do not provide visual information, the intuitive identification of SLNs is challenging [6,7]. On the other hand, blue dye visually stains the lymphatic network, enabling the intuitive identification of SLNs without radiation exposure. However, relying on visual inspection of blue-dyed SLNs may introduce inter-physician variability and potential inaccuracies in identifying SLNs, owing to variable lesion characteristics such as the presence of adipose tissue and blood. These limitations make it challenging to see blue dye within LNs, ultimately leading to reduced sensitivity in the SLN detection [8,9].

Photoacoustic (PA) imaging or sensing is a non-ionizing technique that utilizes the intrinsic light absorption properties of biological tissue components [10–29]. To generate PA signals, a nanosecond pulsed laser induces repeated instantaneous thermal expansions within a sample, creating acoustic waves [30–36]. These acoustic waves are then captured by an ultrasound transducer and analyzed to confirm the presence of specific constituents within the sample [37–43]. PA sensing technology can detect dye-stained LNs with high sensitivity and provide a real-time quantitative representation [44–48]. This method can precisely determine the presence or absence of dyed SLNs that may have been indistinguishable through visual inspection [49–52]. Consequently, it can facilitate SLNb procedures without radioactive materials. In our previous studies, we successfully devised a cutting-edge system known as the photoacoustic finder (PAF), which is remarkably efficacious in detecting SLNs while maintaining a high signal-to-noise ratio (SNR). A recent study by Jiang et al. introduced the Photoacoustic Pen (PAPen) for SLN detection [53]. Unlike PAPen, PAF integrates a solid-state dye (SSD) laser with an articulated arm handpiece and a transparent ultrasound transducer (TUT) in a precisely coaxial configuration. By utilizing the articulated arm to deliver higher laser power, PAF enhances the SNR for PA signal detection [54]. In preclinical studies, the PAF detected blue-dyed rat SLNs through chicken tissue layers up to 18 mm thick. We also subcutaneously injected melanoma into a living mouse and detected it using PAF without a contrast agent, producing strong signals through 18 mm of chicken tissue. These findings support the feasibility of PAF for clinical use.[55]. This PAF has several advantages over conventional SLN detection methods. Unlike radioisotope-based techniques, it eliminates radiation exposure and the need for specialized facilities, making the procedure safer and more accessible while maintaining comparable detection accuracy. PAF also can overcome the limitations of visual inspection, which can be affected by adipose tissue and blood interference, by providing higher specificity and reducing observer variability.

In this cross-sectional clinical study was conducted *ex vivo* to validate the feasibility of using the PAF in a clinical setting. The process confirms the signal from excised LNs identified by the dual-modal method and the PAF before sending them to pathology. To determine its detection performance, the effectiveness of PAF is compared to the detection rate of standard SLNb. The results establish the clinical feasibility of using PAF for SLNb, providing a non-radioactive alternative.

2. Methods

2.1. Study design and participants

This study was conducted as a cross-sectional, open-label, single-arm *ex vivo* study to investigate the efficacy of PAF compared to standard dual-modal methods for SLN detection in the surgery of breast cancer. The SLNb procedures followed international guidelines, using both radioisotope and blue dye mapping. SLNs were identified using gamma probe and blue dye visual inspection, then resected and labeled to reconfirm the with gamma probe and blue dye visual inspection. Subsequently, we employed PAF to capture signals from the LNs. To minimize potential errors such as labeling mistakes and LN delivery errors, the PAF system was placed in the operating room. If patient information or measurement PAF data was missing, we marked the missing patient number and removed it before statistical analysis. The study was conducted continuously until the desired sample size was reached among women diagnosed with breast cancer who met the following inclusion criteria: 1) age between 19 and 74 years, 2) histologically confirmed invasive breast cancer or intraepithelial carcinoma, and 3) no clinical suspicion of axillary LN metastasis. Exclusion criteria included patients who had 1) previously undergone ipsilateral breast or 2) axillary surgery, 3) received chemotherapy prior to surgery, 4) were unable to undergo SLN biopsy, 5) had confirmed axillary LN metastasis by histologic examination, or 6) had breast cancer while lactating or pregnant. Informed consent was obtained prior to procedures, in accordance with the Declaration of Helsinki [56]. This study followed the Strengthening the Reporting of Observational Studies in Epidemiology (STROBE) reporting guidelines for cross-sectional studies (Supplementary Method S1). Regarding bias assessment and management, we categorized potential biases into eight distinct types [57] and systematically evaluated the likelihood of occurrence for each within the context of this study. For biases with a high likelihood of occurrence, we developed and implemented tailored management strategies to mitigate their potential impact. These strategies were applied throughout the study to ensure the reliability and validity of the results (Supplementary Table S1).

2.2. Configuration of the PAF

The PAF consists of a TUT coaxially connected to the handpiece of an SSD laser (COSJET ATR, WONTECH Corp., Republic of Korea) (Fig. 1). The SSD laser converts 532-nm wavelength laser illumination into a 650-nm wavelength that is highly absorbed by blue dye [58,59]. The optical absorption coefficient of blue dye approximately four times larger than that of blood (HbO_2 and HbR) and about 9000 times larger than that of fat, that main component of adipose tissue, resulting in a significant difference in PA signal intensity (Supplementary Figure S1) [60]. Therefore, even when surrounded by adipose tissue, blue-dyed SLNs absorb sufficient light to be clearly distinguished from the surrounding tissue. The laser pulse width is 5 – 40 ns, and the pulse repetition frequency is 5 Hz.

The 650-nm laser beam passes through the TUT coaxially connected to the handpiece and irradiates the LNs. The center frequency of the TUT is 14 MHz, with a 60 % bandwidth. The laser beam passing through the TUT causes an instantaneous thermal expansion of the blue dye molecules in the LN, which immediately contract, generating PA signals. The PA signals are collected by the TUT, amplified by the pulser/receiver (DPR300, JSR Corp., Japan), then digitized and stored in a PC.

2.3. Processing of PAF signal

The PAF detection was performed *ex vivo* after the LNs were removed from the patient's body and before they were sent to the pathology department (Supplementary Movie S1). For accurate analysis, we acquired a background signal and a LN PA signal at that time. The background PA signal was the signal measured in the absence of a LN, whereas the LN PA signal was the signal generated from a LN. To reduce noise, the background and PA LN signals were averaged 5 times each and then bandpass filtered (10 – 22.5 MHz). We demodulated the filtered background and LN PA signals and calculated the difference between the peak value of the PA LN signal and the mean value of the

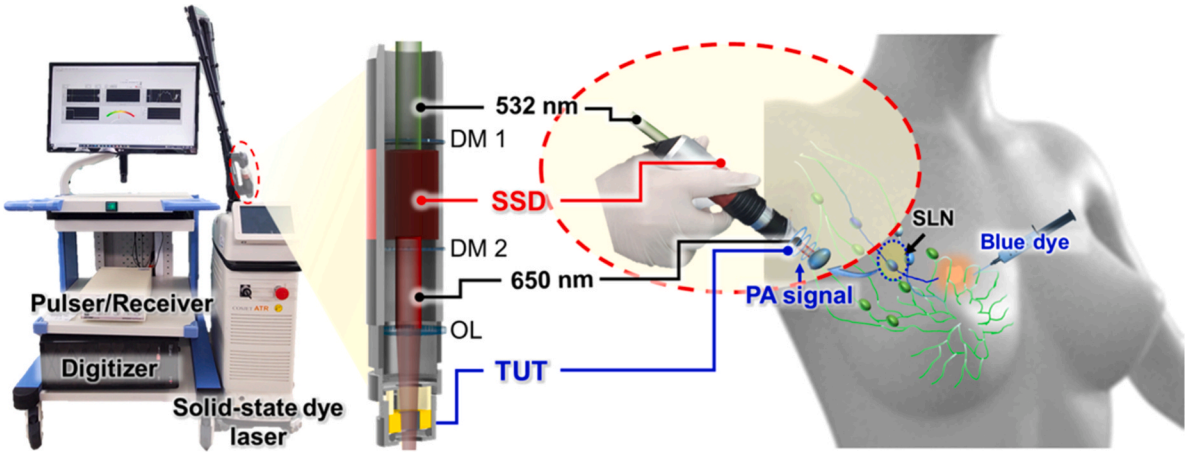

Fig. 1. System configuration and schematic of the PAF. DM, dielectric mirror; OL, objective lens; PA, photoacoustic; PAF, photoacoustic finder; SSD, solid-state dye; and TUT, transparent ultrasound transducer.

background signal (i.e., peak LN PA signal – mean background signal) (Supplementary Figure S2a). Furthermore, we used FFT to plot the frequency response amplitudes of the filtered control and PA LN signals. We calculated the difference between the mean amplitudes of the background and the LN PA spectrum (i.e., the mean LN PA spectrum amplitude minus the mean background spectrum amplitude) (Supplementary Figure S2b). Lastly, we obtained the PAF signal of the LN by calculating the average of both the LN PA amplitude and the LN PA spectrum (Supplementary Figure S2c). We set the detected signal to zero if either of these two values (PA LN amplitude or PA LN spectrum) was less than zero.

2.4. Sentinel lymph node biopsy

The SLNb was performed in accordance with established international guidelines, utilizing both radioisotope and blue dye mapping methods. Five surgical oncologists participated in the study, all of whom were experienced in performing standard dual-modal SLNb and understood the clinical protocol. The radioisotope (0.1 ml of $^{99\,m}$Tc-phytate) was administered into the subdermal lymphatic flexus under the areola within 30 minutes to 8 hours prior to operation. When the surgery started, the operator confirmed the location of the tumor. Then, a blue dye (indigo carmine, 2–5 ml) was injected peritumorally or periareolarly prior to incision, with subsequent massaging for 1 minute following injection. In this study, only indigo carmine was used, as it has been widely utilized in various clinical trials and has been reported to have a low incidence of adverse effects, including anaphylaxis [61]. The axillary nodal basin was closely examined using a handheld gamma probe to detect radioactive signals and visually examined by the naked eye to detect grossly blue-dyed LNs. The identification of SLNs continued until either no further signal was detected by the gamma probe or blue-dyed LNs were no longer found in the nodal basins within the operation field. For this study, SLNs were defined as LNs with a gamma probe signal greater than 10 % of the maximum signal value and/or visibly stained with blue dye. Additionally, based on the surgeon's experience, abnormally palpable LNs that were not detected by gamma probe and visual inspection were also excised, and these were labeled as non-SLNs. The SLNs and non-SLNs were further examined by PAF, and subsequently were forwarded to the pathology department for frozen section analysis (Supplementary Movie S1).

2.5. Study size estimation

To determine the required sample size for testing the non-inferiority of PAF and the dual-modal method, we utilized the non-inferiority chi-square sample size estimator, employing a non-inferiority margin of 5 %, a significance level (alpha) of 5 %, and a power (1-beta) of 80 %. Drawing from prior research and based on experimental data from our tests, we assumed a visual detection rate of approximately 78 % for SLNs [4,62] and 84 % for PAF. Our calculations revealed that a total of 157 SLNs would be necessary [63,64], which corresponds to approximately 1.5 SLNs per patient [6], and hence we would need to enroll 115 patients to fulfill our sample size requirements with an anticipated 10 % drop-out.

2.6. Statistical analysis

The primary endpoints, which were the SLN detection rates for the gamma probe, visual inspection, and PAF were defined as follows:

$$\textit{Detection rate} = \frac{\textit{Number of detected SLNs}}{\textit{Total number of SLNs}} \times 100 \quad [\%]$$

The secondary endpoints encompassed the results of a non-inferiority analysis conducted using the chi-square test. Additionally, we assessed the sensitivity and specificity through receiver operating characteristic (ROC) curve analysis as part of the additional endpoints. Regarding primary and secondary endpoints, we specifically examined SLNs, excluding non-SLNs to minimize potential surgeon subjectivity.

We performed the Wilcoxon Mann-Whitney U-Test to determine the cutoff for the PAF and compared the statistical significances between $^{99\,m}$Tc$^{+/-}$, blue$^{+/-}$, and non-injected groups. In a non-inferiority analysis, we performed a chi-square test to compare the risk differences for $^{99\,m}$Tc^{+}, blue^{+}, and PAF^{+} nodes. We used the independent samples *t*-test for other normal distributions, such as age and body mass index (BMI). All statistical analyses in this study were conducted using MATLAB R2022a with the Statistics and Machine Learning Toolbox.

3. Results

3.1. Study population

A total of 129 patients with breast cancer underwent SLNb over a 14-month period from Jul. 2022 to Sep. 2023. Of these, five patients underwent SLNb using only the radioactive isotope to identify false PA signals from either normal or electrocauterized LNs and nearby tissues (e.g., vessels, lymphatic channels, fat, and muscles). In addition, two patients had failed SLN detection, and one patient had incomplete patient information. As a result, 8 participants were excluded from the analysis due to non-compliance with the study protocol (Fig. 2). Therefore, the data of 121 patients were analyzed. Among these patients, two had bilateral breast cancer and underwent SLNb of each axilla, which were considered separate procedures. Of 121 patients, 220

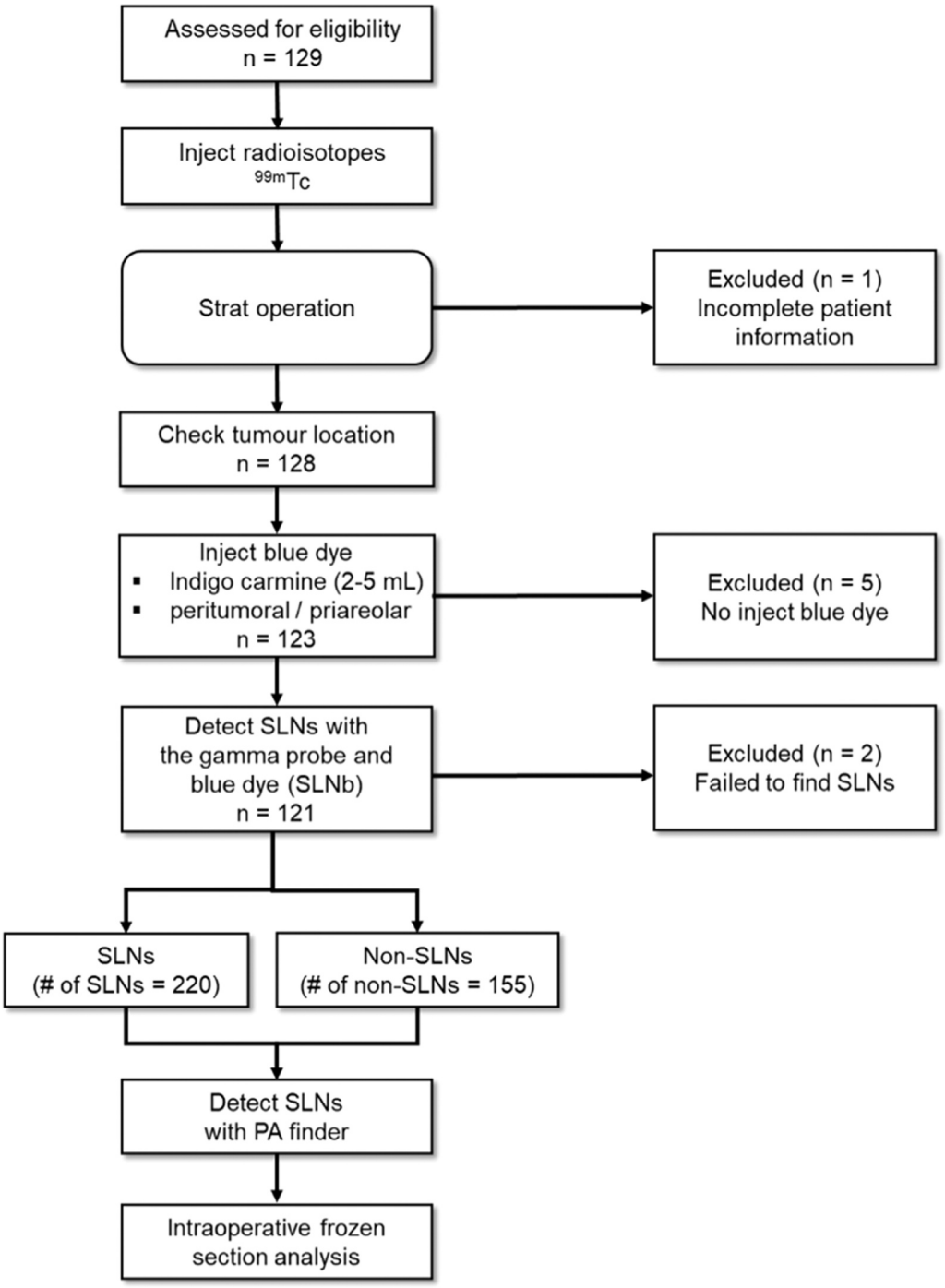

Fig. 2. STROBE flow chart. A total of 129 patients were enrolled, of which 5 patients were excluded for non-injection of blue dye, 1 patient for missing patient information, and 2 patients for SLNb failure. Therefore, we analyzed 121 patients, excluding 8 patients. In the 121 patients, the number of resected SLNs was 220 and the number of non-SLNs was 155. PAF, photoacoustic finder; SLN, sentinel lymph node; SLNb, sentinel lymph node biopsy.

SLNs and 155 non-SLNs were resected, and no complications such as anaphylaxis were observed. The study population had a mean age of 54.03 years and mean body mass index (BMI) of 23.63. The blue dye was injected according to the surgeon's standard practice, with 73 % of the patients receiving 5 ml of blue dye, 8 % receiving 3 ml, and 19 % receiving 2 ml. Despite variation in the injection volume, the concentration of the blue dye (8 mg/ml) remained constant and did not affect the intensity of the PAF signal. The number of sentinel lymph nodes detected was 1.76 ± 1.02 ($n = 89$) for 5 ml, 2.08 ± 1.16 ($n = 11$) for 3 ml, and 1.69 ± 1.06 ($n = 23$) for 2 ml. These differences in sentinel lymph node detection were not statistically significant, with an independent *t*-test p-value > 0.05. These differences in sentinel lymph node detection were not statistically significant (independent *t*-test p-value > 0.05). Breast-conserving surgery was performed in 90 % of the patients, while total mastectomy was performed in 10 %. On an average, 1.82 SLNs were excised per patient, and the mean tumor size was 1.64 cm. The tumor grade distribution was as follows: 26 %, 57 % had grade 2, 12 % had grade 3, and 4 % had grade 1, grade 2, grade 3, and undetermined grades, respectively. Among the SLNs detected, 88 % were without metastasis and 12 % were confirmed to have metastasis (Table 1 and Supplementary Table S2).

Table 1
Characteristics of patients (n = 121).

Characteristic	Value
Age, y, mean (SD)	54.07 (9.53)
BMI, kg/m^2, mean (SD)	23.66 (3.49)
Amount of blue dye, No (%)	
5 ml	87 (72 %)
3 ml	11 (9 %)
2 ml	23 (19 %)
Type of operation, No (%)	
Breast conserving surgery	109 (90 %)
Total mastectomy	12 (10 %)
No. excised SLN, mean (SD)	1.82 (1.04)
Tumor Size, cm, mean (SD)	1.64 (1.08)
Grade, No (%)	
1	32 (26 %)
2	69 (57 %)
3	15 (12 %)
Unknown	5 (4 %)
Status of SLNs, No (%)	
Metastasis	14 (12 %)
No metastasis	107 (88 %)

Abbreviations: BMI, body mass index; SLN, sentinel lymph node; SD, standard deviation; No, number.

3.2. Analysis of PAF signals and performance comparison with visual inspection

To establish a detection criterion for PAF, the PAF signal magnitude was compared in the blue$^+$ nodes (LNs where blue dye was visible to the naked eye), blue$^-$ nodes (LNs without visible blue dye), and no-injection nodes (LNs from patients without blue dye injection) (Supplementary Figure S3). As a result, the PAF signals in the blue$^+$ nodes (95 % CI: 27.79 ~ 35.12 [a.u.]) were found to be significantly higher than those in the blue$^-$ nodes (95 % CI: 10.32 ~ 16.33 [a.u.]) ($p < 0.001$), while there was no statistically significant difference in the PAF signal between the blue$^-$ nodes and no-injection nodes (95 % CI: 1.44 ~ 4.85 [a.u.]) ($p = 0.1$) (Fig. 3a). As for the PAF detection criteria, we established that the PAF signal was present for PAF detection if it exceeded the maximum PAF signal observed in the no-injection nodes, with a cutoff value of 9. PAF measurements for 41 % (88/214) of the blue$^-$ nodes indicated a signal above the cut-off value. These nodes were not detected visually but displayed a faint bluish tinge when the brightness of the photos taken during the PAF measurement was increased (Supplementary Figure S4). Employing the visual inspection results as the gold standard, we computed the sensitivity and specificity across various threshold values of the PAF signal (empirical point), subsequently generating a receiver operating characteristic (ROC) curve that encompasses all LNs. The red point on the ROC curve represents a pre-defined cutoff value (Fig. 3b). At this point, the sensitivity was 1.00, indicating the successful identification of all blue$^+$ nodes by PAF. However, the specificity was 0.59, which was slightly lower because of the PAF's detection of blue$^-$ nodes with faint blue coloring. Despite this, with an area under the curve (AUC) of 0.86, the system demonstrates reasonably fair overall performance[65]. These findings suggest that the PAF system using a cutoff value of 9 for the PAF signal is promising for detecting SLNs, especially in cases where visual inspection is insufficient.

3.3. Performance comparison between gamma probe and PAF

We analyzed the PAF signals of nodes detected by the gamma probe, categorizing them as $^{99\,m}$Tc$^+$ nodes (LNs detected by the gamma probe), $^{99\,m}$Tc$^-$ nodes (LNs undetected by the gamma probe), and no-injection nodes. Among the $^{99\,m}$Tc$^+$ nodes, 68 % (127/186) were visually blue and exhibited elevated PAF signal. While 18 % (34/186) of the $^{99\,m}$Tc$^-$ nodes were visually blue, the majority (82 %, 155/186) were not blue. However, a portion of the $^{99\,m}$Tc$^-$ nodes, although not visibly blue, displayed a slightly blue color when the brightness of the photos was increased and PAF signals were detected (Supplementary Figure S4). The PAF signal of $^{99\,m}$Tc$^+$ nodes (95 % CI: 22.64 ~ 30.16 [a.u.]) was higher than that $^{99\,m}$Tc$^-$ nodes (95 % CI: 12.72 ~ 15.85 [a.u.]) ($p < 0.001$), and $^{99\,m}$Tc$^-$ nodes exhibited higher signals than the no-injection nodes (95 % CI: 1.44 ~ 4.85 [a.u.]) ($p = 0.02$) (Fig. 3c). Additionally, we plotted an ROC curve for all LNs, using the gamma probe as the gold standard instead of visual inspection and found a sensitivity of 0.79 and specificity of 0.51 at the cutoff value; the AUC was 0.71 (Fig. 3d). These results suggest that although the PAF system demonstrated a sensitivity and specificity comparable to those of the gamma probe, compared to using visual inspection as the gold standard, it had a lower sensitivity and specificity and a smaller AUC when detecting SLNs. This discrepancy can be attributed to differences in tracer detection between the gamma probe and visual inspection.

3.4. Comparison of PAF and the standard dual-modal detection method

After confirming the efficiency of the system in detecting SLNs, our investigation was expanded to include all LNs, including nonSLNs. Non-SLNs are LNs located within the resected LN mass, not identified by dual-modal methods (gamma probe and visual inspection), but palpable during surgery. Comparing the PAF signals in SLNs and non-SLNs, we observed a significant increase in the PAF signal in SLNs (95 % CI: 23.55 ~ 30.21 [a.u.]) than in non-SLNs (95 % CI: 7.08 ~ 11.00 [a.u.]) ($p < 0.001$) (Fig. 3e). Using the dual-modal method as the gold standard, the ROC curve displayed a sensitivity of 0.81 and a specificity of 0.63 for PAF (Fig. 3f). The sensitivity, at 0.81, was lower than that achieved with visual inspection as the gold standard (1.00), yet higher than that with the gamma probe (0.79). These findings indicated that some non-SLNs emitted a faint blue color, undetected by visual inspection, but were still identified by the PAF. The specificity, at 0.63, surpasses those of both visual inspection and the gamma probe when dual-modal methods are used as the gold standard, demonstrating the effectiveness of the PAF in detecting faint blue nodes. Interestingly, 37 % (58/155) of the non-SLNs showed a PAF signal above the pre-defined cut-off value. Given the proximity of non-SLNs to SLNs in the LN mass, it is presumed that the non-SLNs contained blue dye, which was visually indistinguishable due to the surrounding adipose tissue and was detected only by PAF. These findings indicate that the PAF system not only performs well in detecting SLNs, but also shows promise in identifying non-SLNs that may contain blue dye but are visually indistinguishable.

3.5. Primary endpoint: comparative analysis of SLN detection rates for PAF, gamma probe, and visual inspection

SLNs were identified using gamma probes, visual inspection, and PAF. To evaluate the SLN detection rate of each method, we calculated their respective detection rates, considering the detection rate as the primary endpoint of the analysis. To ensure a fair comparison between the systems, non-SLNs (palpable LNs) were excluded from this calculation. Of the 220 SLNs, 87 % (191/220) were detected by PAF and 85 % (186/220) were detected using the gamma probe. Table 2 shows that 73 % (161/220) of the nodes were identified as blue nodes through visual inspection. In addition, a total of 14 patients in the study had histologically confirmed metastatic cancer in SLNs, with the gamma probe and PAF showing a 100 % (14/14) detection rate in patients with metastatic SLNs, and blue dye visual inspection showing a 79 % (11/14) detection rate (Table 2 and Supplementary Table S3).

We then compared and analyzed the SLN detection rates for each method. A total of 84 % (157/186) of $^{99\,m}$Tc$^+$ nodes were confirmed by PAF, whereas only 68 % (127/186) of $^{99\,m}$Tc$^+$ nodes were identified during visual inspection with blue dye. In addition, 100 % (161/161) of the blue$^+$ nodes were identified using PAF, whereas 79 % (127/161) of the blue$^+$ nodes were detected using the gamma probe (Table 2). These findings indicate that PAF performs comparably to the gamma probe

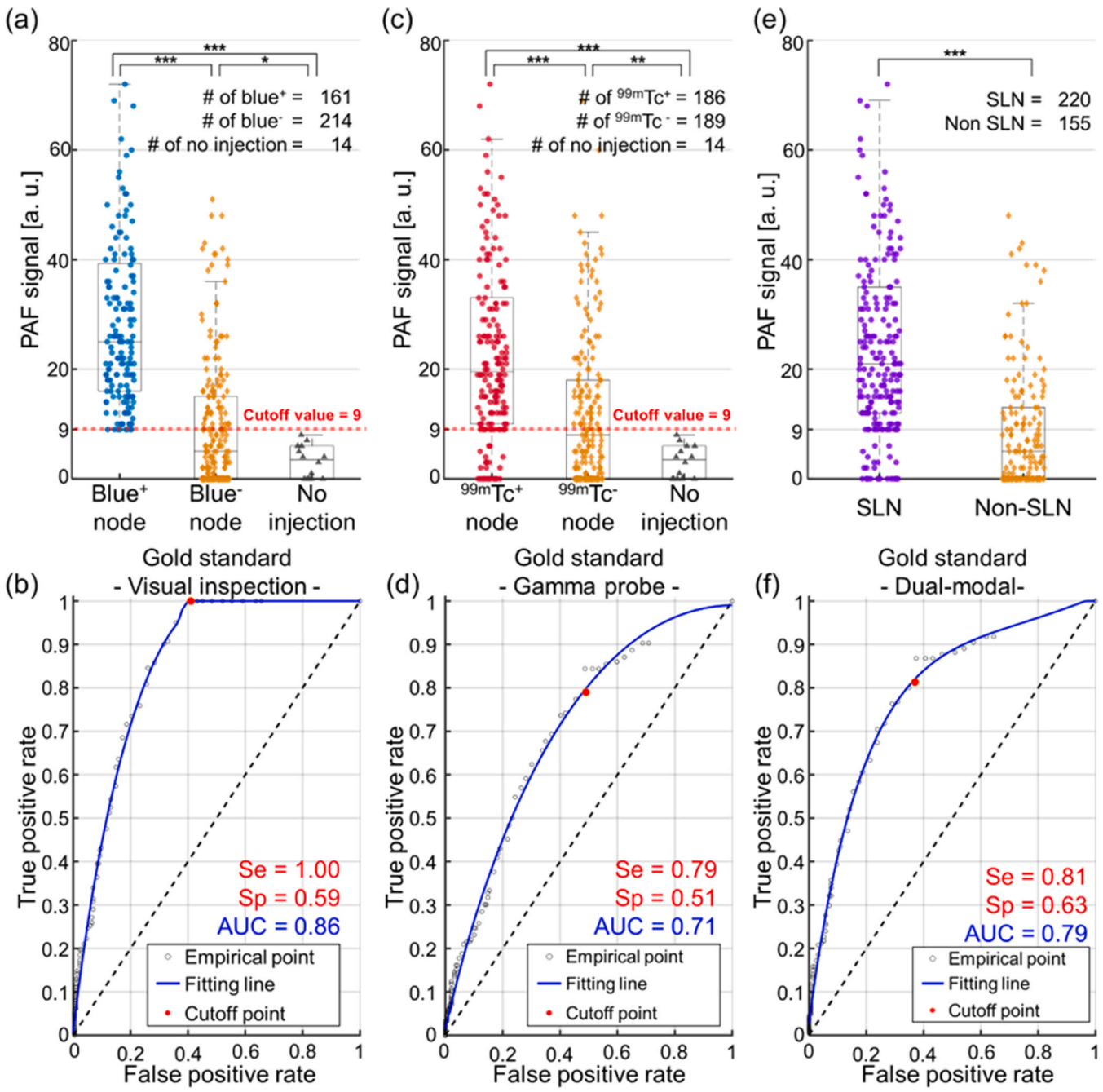

Fig. 3. Comparison of PAF signals for each node. (a) Comparison of PAF signals of blue+ /- nodes and no injection nodes. Categories of LNs: blue+ nodes, LNs stained with blue dye; blue- nodes, LNs not stained with blue dye; no-injection nodes, LNs from patients who did not receive blue dye. (b) The ROC curve utilized visual inspection as the gold standard. The red point is the cutoff point (Cutoff value = 9). (c) Comparison of PAF signal of 99mTc+ /- nodes and no injection nodes. Categories of LNs: 99mTc+ nodes, LNs detected by gamma probe; 99mTc- nodes, LNs undetected by gamma probe; no-injection nodes, LNs from patients who did not receive blue dye (d) The ROC curve utilized gamma probe detection as the gold standard. (e) Comparison of the PAF signals of SLNs and non-SLNs. (f) ROC curves with the dual-modal method as the gold standard. Red indicates the cutoff point. PAF, photoacoustic finder; SLN, sentinel lymph node; PA, photoacoustic; ROC, receiver operating characteristic; Se, sensitivity; Sp, specificity; and AUC, area under the curve; * ** , $p < 0.001$; * *, $p < 0.05$; * , $p < 0.1$.

and surpasses visual inspection. Moreover, it exhibits substantial concordance with the SLNs identified by the gamma probe, in contrast to visual inspection.

3.6. Secondary endpoint: non-inferiority analysis for PAF vs. gamma probe and visual inspection

As a second endpoint, we performed a non-inferiority analysis using a chi-square test to ensure that the detection capability of the PAF was not inferior to that of the gamma probe and visual inspection, setting the absolute margin of non-inferiority at 5 %. This analysis utilized the previously obtained SLN detection rates. The risk difference between the gamma probe and PAF was calculated to be −2.27 % (95 % CI: −8.81 % ~ 4.27 %), confirming PAF's non-inferiority of PAF ($p = 0.015$) (Fig. 4). Furthermore, the risk difference between visual inspection and PAF was determined to be −13.64 % (95 % CI: −21.00 % ~ −6.27 %), further reinforcing the superiority of PAF to visual inspection ($p < 0.001$). These results demonstrated PAF's ability of PAF to consistently match or

Table 2
SLN detection rate for each method.

Method	Detection rates					
	Total SLNs (n = 220)[a]	Each node[b]				Metastatic patients (n = 14)[c]
		$^{99m}Tc^{+}$ (n = 186)	$^{99m}Tc^{-}$ (n = 34)	$Blue^{+}$ (n = 161)	$Blue^{-}$ (n = 59)	
Gamma probe	85 % (186/220)	100 % (186/186)	0 % (0/34)	79 % (127/161)	100 % (59/59)	100 % (14/14)
Visual inspection	73 % (161/220)	68 % (127/186)	100 % (34/34)	100 % (161/161)	0 % (0/59)	79 % (11/14)
PAF	87 % (191/220)	84 % (157/186)	100 % (34/34)	100 % (161/161)	51 % (30/59)	100 % (14/14)

Abbreviations: CI, confidence interval; RD, risk difference
[a] Detection rate of SLN (SLN: $^{99m}Tc^{+}$ or $Blue^{+}$)
[b] Detection rate of each node
[c] Number of metastatic patients

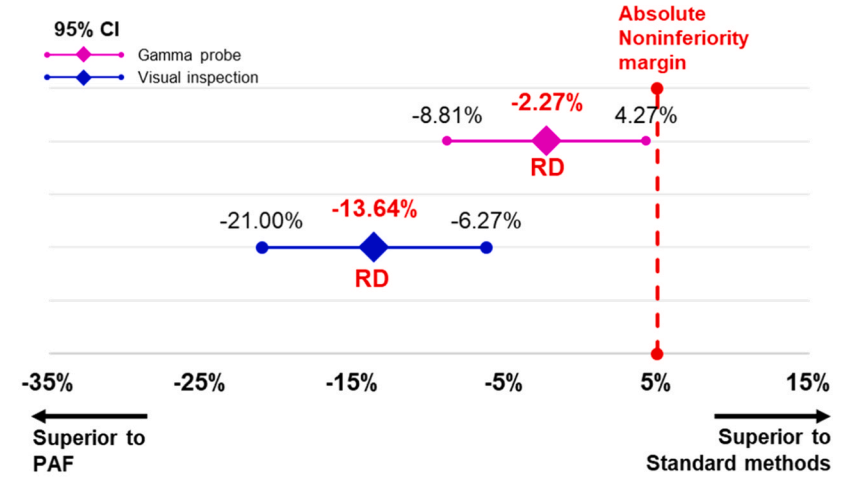

Method	Noninferiority analysis		
	RD	95% CI	P-value
Gamma probe	-2.27	- 8.81~ 4.27	0.015
Visual inspection	-13.64	- 21 ~ - 6.27	< 0.001

Fig. 4. Analyzing the non-inferiority of PAF to the gamma probe and visual inspection. CI, confidence interval; RD, risk difference.

exceed the performance of standard SLN detection methods, emphasizing its reliability and potential as an alternative to SLN detection.

4. Discussion

The detection of SLNs using a gamma probe with radioactive materials poses numerous challenges, including concerns regarding radiation exposure, contamination risks, equipment costs, proper waste disposal, and regulatory compliance. Despite these limitations, radioactive materials and blue dyes are commonly used to improve the detection rate of SLNb. In particular, blue dye is often the preferred option in hospitals without access to nuclear medicine equipment. Our study aimed to explore the potential of PAF as a method to detect SLNs without the need for advanced technology such as nuclear medicine.

This study assessed the effectiveness of the PAF system by comparing the detection rates of the gamma probe, blue dye visual inspection, and PAF for SLN detection. The results revealed comparable detection rates of 87 % (191/220) for the PAF probe and 85 % (186/220) for the gamma probe, with visual inspection lagging at 73 % (161/220). These findings indicate that the PAF system performs similarly to the gamma probe and surpasses visual inspection in terms of its effectiveness. Moreover, in patients with histologically confirmed metastatic cancer in the SLN, blue dye visual inspection achieved a 79 % (11/14) identification rate, whereas both the gamma probe and PAF demonstrated a 100 % (14/14) detection rate. This performance underscores the efficiency of PAF in ensuring that no metastatic cases are overlooked, potentially leading to improved patient care and informed surgical decisions. A non-inferiority analysis comparing the PAF's detection capability with those of the gamma probe and visual inspection, using a 5 % non-inferiority margin, showed that PAF had a risk difference of −2.27 % (95 % CI: −8.81 % ~ 4.27 %) compared to the gamma probe ($p = 0.015$). Additionally, the risk difference between visual inspection and PAF was −13.64 % (95 % CI: −21.00 % ~ −6.27 %), further highlighting PAF's superiority of PAF over visual inspection ($p < 0.001$). These findings emphasize the efficacy of PAF as a non-ionizing alternative to gamma probes for SLN detection in breast cancer surgery, alleviating the concerns associated with conventional methods.

The effectiveness of PAF in detecting SLNs is attributed to its heightened sensitivity to blue dyes. PAF demonstrated a flawless detection rate of 100 % (161/161) among all LNs identified during blue dye visual inspection, highlighting PAF's remarkable ability of PAF to

precisely identify SLNs when the blue dye is visually apparent. The PAF signal from the blue^{+} nodes was significantly more pronounced than that from the blue^{-} nodes ($p < 0.001$). Additionally, PAF detected 41 % (88/214) of the blue^{-} nodes, where LNs exhibited a bluish appearance upon increasing the brightness of the photographs (Supplementary Figure S1). This observation suggests that blue dye might be present within LNs, but not clearly visible to the naked eye, due to factors such as the low concentration of the dye or the presence of a layer of fat covering the LNs[66]. Furthermore, PAF successfully identified 84 % (157/186) of $^{99m}Tc^{+}$ nodes. Although this detection rate surpasses the 68 % (127/186) achieved through visual inspection, a 16 % uncertainty persisted. This uncertainty may stem from the distinctive characteristics of the tracers used by the gamma probe and the PAF. The gamma probe relies on the detection of a radioactive tracer, whereas the PAF utilizes the PA signal emitted by the blue dye. Notably, the radiotracer and blue dye are administered at different times due to variations in their lymphatic transit rates and injection sites [67–69]. Moreover, the indigo carmine blue dye used in this study exhibited a relatively low protein affinity compared to other blue dyes, leading to a significant portion diffusing into the surrounding microvasculature [69]. As a result, it is possible that the blue dye did not reach the same location as the radioisotope tracer.

When comparing PAF signals in SLNs and non-SLNs, we observed a significant increase in the PAF signal in SLNs (95 % CI: 23.55 ~ 30.21 [a.u.]) than in non-SLNs (95 % CI: 7.08 ~ 11.00 [a.u.]) ($p < 0.001$). Interestingly, a PAF signal was detected in 37 % (58/155) of non-SLNs. When the brightness of the photos of non-SLNs with an identified PAF signal increased, faint blue staining was observed (Supplementary Figure S1). We attempted to confirm the presence of blue dye by visual inspection of frozen sections, but the dye was not distinctly visible in the sections (Supplementary Figure S5). The absence of blue dye in the frozen section may be due to loss during the washing of the surrounding tissue that accompanies the LNs in preparation for the frozen section. Consequently, in this study, we assumed that all LNs not detected by the dual-modal methods were false positives. PAF exhibited a slightly lower performance, with a sensitivity of 81 % and a specificity of 63 %. However, considering that PAF detected all SLNs identified by visual inspection and 84 % of the $^{99m}Tc^{+}$ nodes and given the anatomical proximity of non-SLNs to SLNs, it is plausible that blue dye was present in the nodes detected by PAF, suggesting the potential for higher performance of the PAF system.

Beyond tracer properties, the differences in detection rates between gamma probes and PAF may stem from the limitations of current PAF systems. It is crucial to acknowledge that distinguishing the PAF signal from the blue dye may face constraints owing to background signal interference. Two approaches can be applied to address this concern: 1) multiple wavelengths can be employed to enhance the sensitivity of PAF by facilitating precise identification of PA signals from blue dyes through spectral unmixing. Although only the 650 nm wavelength was used in this study due to laser limitations, we have developed a dual-wavelength laser (650 nm and 1064 nm) and are currently in the process of certifying it. The use of these two wavelengths will improve the SNR and enable deeper signal detection, providing better differentiation between blue dye signals and background noise. Once certified, we will use this laser in future clinical studies to enhance blue dye detection specificity. 2) A low-frequency TUT can be used to increase the detection sensitivity. The current PAF system utilizes a TUT with a high center frequency of 14 MHz. In soft tissues, the attenuation coefficient is approximately 0.75 dB/cm/MHz [70], meaning a 14 MHz signal experiences about 10.5 dB of attenuation per centimeter of tissue. When using a lower frequency TUT, such as 8 MHz, the attenuation per centimeter of tissue is approximately 3.75 dB, allowing the signal to penetrate deeper than a 14 MHz TUT. At the time of this study, fabricating a low-frequency TUT with high optical transparency was a challenge, and since this study measured signals from LNs that were excised, 14 MHz TUT was sufficient to receive PA signals. However, the use of a low-frequency TUT is needed to improve measurable sensing depth for future in vivo clinical study. Notably, recent advances in transparent piezoelectric materials have enabled the creation of low-center-frequency TUTs with high optical transmittance using a relatively thick piezoelectric layer [71,72]. We plan to switch from high-frequency TUT to low-frequency TUT for future in vivo clinical study.

This study's relatively small sample size makes it difficult to fully assess the clinical utility of PAF based on this study alone. However, it is important to note that this pilot study was designed to explore the feasibility of PAF technology. We believe that the promising results observed in this pilot study lay the groundwork for further validation through larger clinical trials. Another consideration is the utility of PAF in the context of advancements in minimally invasive techniques, such as advanced endoscopic methods[73–75]. Despite these advances, many hospitals still rely on conventional SLN detection methods, like the use of blue dye, due to limited access to advanced surgical equipment. In such settings, PAF can enhance the accuracy of SLN detection when blue dye alone does not provide clear visual identification. Additionally, PAF systems and gamma probes have similar acquisition costs, but PAF systems do not require radioactive materials or complex facilities, making them more feasible for hospitals without access to advanced systems or nuclear medicine equipment.

Finally, the PAF used in the study was operated ex vivo, as it has not yet received certification from the local government. Hence, measuring the signal with PAF while the LNs were within the body was unfeasible. Despite conducting PAF detection in the operating room promptly after SLN dissection for accurate comparison of PAF evaluation results, potential discrepancies may arise between in vivo SLNb (i.e., a gamma probe and blue dye visual inspection) and ex vivo PAF evaluation. However, the blue dye measured by the PAF system provides significantly more contrast than blood and adipose tissue (Supplementary Figure S1). To further ensure detection accuracy, we used the maximum PAF signal value identified in SLNs from patients without blue dye injection as a cut-off value. Only LNs with a PAF signal exceeding this cut-off, i.e., greater than the PAF signal from blood, were considered to contain blue dye and thus identified as SLNs. Therefore, we anticipate minimal differences in accuracy between in vitro and in vivo conditions. Nevertheless, we recognize the importance of further in vivo testing to validate our findings. We are currently pursuing certification for in vivo experimentation with PAF, and hope to conduct further investigations in the future.

In conclusion, this study investigated the clinical feasibility of PAF for SLN detection in patients with BC. Comprising an SSD laser and a TUT, the PAF is portable and well suited for operating room integration. By utilizing TUT and SSD coaxial structures and wavelengths that match the optical absorption characteristics of blue dye, we effectively detected blue-dyed SLNs with high sensitivity. Comparing the detection rate of SLNs to the standard dual-modal method of gamma probe and blue dye visual inspection, the PAF achieved a detection rate of 87 %, which is on par with that of the gamma probe (85 %) and superior to that of visual inspection (73 %). We also confirmed that PAF is non-inferior to dual-modal detection by conducting a non-inferiority test ($p < 0.001$) for SLN detection in all resected LNs. These findings suggest that PAF holds promise as a potential alternative to the standard dual-modal method of SLN detection, paving the way for future SLN detection using blue dye alone, without the need for radioactive materials.

CRediT authorship contribution statement

Ahn Junho: Methodology, Investigation. **Lee Young Joo:** Writing – original draft, Validation, Investigation, Formal analysis, Data curation. **Kim Chulhong:** Writing – review & editing, Supervision, Resources, Investigation, Funding acquisition, Conceptualization. **Ahn Joongho:** Software. **Park Jeongwoo:** Resources. **Nam Sunghun:** Methodology, Investigation, Formal analysis. **Kim Minseong:** Methodology,

Investigation. **Kim Dooreh:** Writing – review & editing, Validation, Supervision, Formal analysis. **Park Byullee:** Writing – review & editing, Writing – original draft, Validation, Conceptualization. **Seo Youngseok:** Resources. **Ryu Hanyoung:** Resources. **Han Moongyu:** Writing – original draft, Visualization, Software, Investigation, Formal analysis, Conceptualization.

Declaration of Competing Interest

The authors declare that they have no known competing financial interests or personal relationships that could have appeared to influence the work reported in this paper.

Acknowledgements

This work was supported in part by the National Research Foundation of Korea (NRF) grant funded by the Ministry of Science and ICT (MSIT) (2023R1A2C3004880), by the Basic Science Research Program through the NRF funded by the Ministry of Education (No. 2020R1A6A1A03047902), by the Korea Medical Device Development Fund grant funded by the Korea government (the Ministry of Trade, Industry and Energy) (Project Number: 1711195277, RS-2020-KD000008), by a grant of the Korea Health Technology R&D Project through the Korea Health Industry Development Institute (KHIDI) funded by the Ministry of Health & Welfare (RS-2024–00512879), by the BK21 Four project, and by the Glocal 30 University Project.

Data availability

Data will be made available on request.

References

[1] D.N. Krag, The sentinel node for staging breast cancer: current review, Breast Cancer 6 (1999) 233–236.
[2] P.J. Borgstein, R. Pijpers, E.F. Comans, et al., Sentinel lymph node biopsy in breast cancer: guidelines and pitfalls of lymphoscintigraphy and gamma probe detection, J. Am. Coll. Surg. 186 (3) (1998) 275–283.
[3] S. Wallace, L. Jackson, B. Schaffer, et al., Lymphangiograms: their diagnostic and therapeutic potential, Radiology 76 (2) (1961) 179–199.
[4] D.N. Krag, S.J. Anderson, T.B. Julian, et al., Technical outcomes of sentinel-lymph-node resection and conventional axillary-lymph-node dissection in patients with clinically node-negative breast cancer: results from the NSABP B-32 randomised phase III trial, Lancet Oncol. 8 (10) (2007) 881–888.
[5] B.E. Schaafsma, F.P.R. Verbeek, D.D.D. Rietbergen, et al., Clinical trial of combined radio-and fluorescence-guided sentinel lymph node biopsy in breast cancer, Br. J. Surg. 100 (8) (2013) 1037–1044.
[6] M. Ahmed, A.D. Purushotham, M. Douek, Novel techniques for sentinel lymph node biopsy in breast cancer: a systematic review, Lancet Oncol. 15 (8) (2014) e351–e362.
[7] J.R. Van der Vorst, B.E. Schaafsma, F.P.R. Verbeek, et al., Randomized comparison of near-infrared fluorescence imaging using indocyanine green and 99 m technetium with or without patent blue for the sentinel lymph node procedure in breast cancer patients, Ann. Surg. Oncol. 19 (2012) 4104–4111.
[8] S. Yamamoto, N. Maeda, K. Yoshimura, et al., Intraoperative detection of sentinel lymph nodes in breast cancer patients using ultrasonography-guided direct indocyanine green dye-marking by real-time virtual sonography constructed with three-dimensional computed tomography-lymphography, Breast 22 (5) (2013) 933–937.
[9] T. Sugie, T. Sawada, N. Tagaya, et al., Comparison of the indocyanine green fluorescence and blue dye methods in detection of sentinel lymph nodes in early-stage breast cancer, Ann. Surg. Oncol. 20 (2013) 2213–2218.
[10] L.V. Wang, J. Yao, A practical guide to photoacoustic tomography in the life sciences, Nat. Methods 13 (8) (2016) 627–638.
[11] J. Weber, P.C. Beard, S.E. Bohndiek, Contrast agents for molecular photoacoustic imaging, Nat. Methods 13 (8) (2016) 639–650.
[12] L.V. Wang, Multiscale photoacoustic microscopy and computed tomography, Nat. Photonics 3 (9) (2009) 503–509.
[13] C. Kim, K.H. Song, F. Gao, et al., Sentinel lymph nodes and lymphatic vessels: noninvasive dual-modality in vivo mapping by using indocyanine green in rats—volumetric spectroscopic photoacoustic imaging and planar fluorescence imaging, Radiology 255 (2) (2010) 442–450.
[14] T.N. Erpelding, C. Kim, M. Pramanik, et al., Sentinel lymph nodes in the rat: noninvasive photoacoustic and US imaging with a clinical US system, Radiology 256 (1) (2010) 102–110.
[15] C. Kim, T.N. Erpelding, L. Jankovic, et al., Performance benchmarks of an array-based hand-held photoacoustic probe adapted from a clinical ultrasound system for non-invasive sentinel lymph node imaging, Philos. Trans. R. Soc. A: Math., Phys. Eng. Sci. 369 (1955) (2011) 4644–4650.
[16] W.J. Akers, W.B. Edwards, C. Kim, et al., Multimodal sentinel lymph node mapping with single-photon emission computed tomography (SPECT)/computed tomography (CT) and photoacoustic tomography, Transl. Res. 159 (3) (2012) 175–181.
[17] M. Kim, J. Kim, D. VanderLaan, et al., Tunable Interparticle Connectivity in Gold Nanosphere Assemblies for Efficient Photoacoustic Conversion, Adv. Funct. Mater. (2023) 2305202.
[18] D.Y. Santiesteban, K.A. Hallam, S.K. Yarmoska, et al., Color-coded perfluorocarbon nanodroplets for multiplexed ultrasound and photoacoustic imaging, Nano Res. 12 (2019) 741–747.
[19] A. Karlas, N. Katsouli, N.-A. Fasoula, et al., Multiscale optoacoustic assessment of skin microvascular reactivity in carotid artery disease, Photoacoustics 40 (2024) 100660.
[20] J. Kim, D. Heo, S. Cho, et al., Enhanced dual-mode imaging: Superior photoacoustic and ultrasound endoscopy in live pigs using a transparent ultrasound transducer, Sci. Adv. 10 (47) (2024) 9960.
[21] D. Kim, E. Park, J. Park, et al., An ultraviolet-transparent ultrasound transducer enables high-resolution label-free photoacoustic histopathology, Laser Photonics Rev. 18 (2) (2024) 2300652.
[22] A.V. Nikolaev, Y. Fang, J. Essers, et al., Pre-transplant kidney quality evaluation using photoacoustic imaging during normothermic machine perfusion, Photoacoustics 36 (2024) 100596.
[23] H. He, C. Fischer, U. Darsow, et al., Quality control in clinical raster-scan optoacoustic mesoscopy, Photoacoustics 35 (2024) 100582.
[24] D. Kim, J. Ahn, D. Kim, et al., Quantitative volumetric photoacoustic assessment of vasoconstriction by topical corticosteroid application in mice skin, Photoacoustics 40 (2024) 100658.
[25] Z. Liang, S. Zhang, Z. Liang, et al., Deep learning acceleration of iterative model-based light fluence correction for photoacoustic tomography, Photoacoustics 37 (2024) 100601.
[26] X. Song, X. Zou, K. Zeng, et al., Multiple diffusion models-enhanced extremely limited-view reconstruction strategy for photoacoustic tomography boosted by multi-scale priors, Photoacoustics 40 (2024) 100646.
[27] J. Yang, S. Choi, J. Kim, et al., Multiplane Spectroscopic Whole-Body Photoacoustic Computed Tomography of Small Animals In Vivo, Laser Photonics Rev. (2024) 2400672.
[28] J. Kim, J. Lee, S. Choi, et al., 3d multiparametric photoacoustic computed tomography of primary and metastatic tumors in living mice, ACS nano 18 (28) (2024) 18176–18190.
[29] C. Lee, S. Cho, D. Lee, et al., Panoramic volumetric clinical handheld photoacoustic and ultrasound imaging, Photoacoustics 31 (2023) 100512.
[30] C. Kim, T.N. Erpelding, K. Maslov, et al., Handheld array-based photoacoustic probe for guiding needle biopsy of sentinel lymph nodes, -4, J. Biomed. Opt. 15 (4) (2010) 046010. -4.
[31] W.J. Akers, C. Kim, M. Berezin, et al., Noninvasive photoacoustic and fluorescence sentinel lymph node identification using dye-loaded perfluorocarbon nanoparticles, ACS nano 5 (1) (2011) 173–182.
[32] C. Smith, J. Shepherd, G. Renaud, et al., Vector-flow imaging of slowly moving ex vivo blood with photoacoustics and pulse-echo ultrasound, Photoacoustics 38 (2024) 100602.
[33] S. Paul, H.S. Patel, V. Misra, et al., Numerical and in vitro experimental studies for assessing the blood hematocrit and oxygenation with the dual-wavelength photoacoustics, Photoacoustics 39 (2024) 100642.
[34] P. Zhang, J. Lv, C. Ge, et al., Quantitative evaluation of microenvironmental changes and efficacy of cupping therapy under different pressures based on photoacoustic imaging, Photoacoustics 40 (2024) 100661.
[35] E. Park, S. Misra, D.G. Hwang, et al., Unsupervised inter-domain transformation for virtually stained high-resolution mid-infrared photoacoustic microscopy using explainable deep learning, Nat. Commun. 15 (1) (2024) 10892.
[36] J. Kim, J.Y. Kweon, S. Choi, et al., Non-Invasive Photoacoustic Cerebrovascular Monitoring of Early-Stage Ischemic Strokes In Vivo, Adv. Sci. (2024) 2409361.
[37] W. Choi, B. Park, S. Choi, et al., Recent Advances in Contrast-Enhanced Photoacoustic Imaging: Overcoming the Physical and Practical Challenges, Chem. Rev. (2023) 2659–2665.
[38] L. Song, C. Kim, K. Maslov, et al., High-speed dynamic 3D photoacoustic imaging of sentinel lymph node in a murine model using an ultrasound array, Med. Phys. 36 (8) (2009) 3724–3729.
[39] J. Koo, M. Jeon, Y. Oh, et al., In vivo non-ionizing photoacoustic mapping of sentinel lymph nodes and bladders with ICG-enhanced carbon nanotubes, Phys. Med. Biol. 57 (23) (2012) 7853.
[40] X. Liu, W.C. Law, M. Jeon, et al., Cu2–xSe nanocrystals with localized surface plasmon resonance as sensitive contrast agents for in vivo photoacoustic imaging: Demonstration of sentinel lymph node mapping, Adv. Healthc. Mater. 2 (7) (2013) 952–957.
[41] S. Tzoumas, A. Nunes, I. Olefir, et al., Eigenspectra optoacoustic tomography achieves quantitative blood oxygenation imaging deep in tissues, Nat. Commun. 7 (1) (2016) 12121.
[42] V. Ntziachristos, D. Razansky, Molecular imaging by means of multispectral optoacoustic tomography (MSOT), Chem. Rev. 110 (5) (2010) 2783–2794.
[43] C. Yoon, E. Park, S. Misra, et al., Deep learning-based virtual staining, segmentation, and classification in label-free photoacoustic histology of human specimens, Light.: Sci. Appl. 13 (1) (2024) 226.

[44] L. Gu, H. Deng, Y. Bai, et al., Sentinel lymph node mapping in patients with breast cancer using a photoacoustic/ultrasound dual-modality imaging system with carbon nanoparticles as the contrast agent: a pilot study, Biomed. Opt. Express 14 (3) (2023) 1003–1014.
[45] I. Stoffels, S. Morscher, I. Helfrich, et al., "Metastatic status of sentinel lymph nodes in melanoma determined noninvasively with multispectral optoacoustic imaging,", Sci. Transl. Med. 7 (317) (2015) 1946–6234.
[46] C. Kim, K.H. Song, L.V. Wang, Sentinel lymph node detection ex vivo using ultrasound-modulated optical tomography, J. Biomed. Opt. 13 (2) (2008) 020507.
[47] K.H. Song, C. Kim, K. Maslov, et al., Noninvasive in vivo spectroscopic nanorod-contrast photoacoustic mapping of sentinel lymph nodes, Eur. J. Radiol. 70 (2) (2009) 227–231.
[48] J. Park, B. Park, U. Yong, et al., Bi-modal near-infrared fluorescence and ultrasound imaging via a transparent ultrasound transducer for sentinel lymph node localization, Opt. Lett. 47 (2) (2022) 393–396.
[49] M. Han, W. Choi, J. Ahn, et al., In vivo dual-modal photoacoustic and ultrasound imaging of sentinel lymph nodes using a solid-state dye laser system, Sensors 20 (13) (2020) 3714.
[50] G.P. Luke, J.N. Myers, S.Y. Emelianov, et al., Sentinel lymph node biopsy revisited: ultrasound-guided photoacoustic detection of micrometastases using molecularly targeted plasmonic nanosensors, Cancer Res. 74 (19) (2014) 5397–5408.
[51] D.S. Dumani, I.-C. Sun, S.Y. Emelianov, Ultrasound-guided immunofunctional photoacoustic imaging for diagnosis of lymph node metastases, Nanoscale 11 (24) (2019) 11649–11659.
[52] L.M.A. Crane, G. Themelis, R.G. Pleijhuis, et al., Intraoperative multispectral fluorescence imaging for the detection of the sentinel lymph node in cervical cancer: a novel concept, %@ 1536-1632, Mol. Imaging Biol. 13 (2011) 1043–1049. %@ 1536-1632.
[53] D. Jiang, J. Zhao, Y. Zhang *et al.*, "Integrated Photoacoustic Pen for Breast Cancer Sentinel Lymph Node Detection." 1-3.
[54] J. Park, B. Park, T.Y. Kim, et al., Quadruple ultrasound, photoacoustic, optical coherence, and fluorescence fusion imaging with a transparent ultrasound transducer, Proc. Natl. Acad. Sci. 118 (11) (2021) e1920879118.
[55] B. Park, M. Han, J. Park, et al., A photoacoustic finder fully integrated with a solid-state dye laser and transparent ultrasound transducer, Photoacoustics 23 (2021) 100290.
[56] A. World Medical, World Medical Association Declaration of Helsinki: Ethical Principles for Medical Research Involving Human Subjects, JAMA 310 (20) (2013) 2191–2194.
[57] J.X. Lambert, [Statistics in brief: how to assess bias in clinical studies?] LWW, (2011).
[58] A. Costela, I. García-Moreno, R. Sastre, Solid-state dye lasers, Tunable Laser Appl. 2 (2009).
[59] A. Costela, I. García-Moreno, R. Sastre, Polymeric solid-state dye lasers: Recent developments, Phys. Chem. Chem. Phys. 5 (21) (2003) 4745–4763.
[60] J. Park, S. Choi, F. Knieling, et al., Clinical translation of photoacoustic imaging, Nat. Rev. Bioeng. (2024).
[61] M. Perenyei, Z.E. Barber, J. Gibson, et al., Anaphylactic reaction rates to blue dyes used for sentinel lymph node mapping: systematic review and meta-analysis, Ann. Surg. 273 (6) (2021) 1087–1093.
[62] J. Guo, H. Yang, S. Wang, et al., Comparison of sentinel lymph node biopsy guided by indocyanine green, blue dye, and their combination in breast cancer patients: a prospective cohort study, World J. Surg. Oncol. 15 (2017) 1–7.
[63] L. Flight, S.A. Julious, Practical guide to sample size calculations: non-inferiority and equivalence trials, Pharm. Stat. 15 (1) (2016) 80–89.
[64] H.J. Lee, Y.S. Kim, I. Park, Calculation of sample size in clinical trials, Clin. Shoulder Elb. 16 (1) (2013) 53–57.
[65] J.N. Mandrekar, Receiver operating characteristic curve in diagnostic test assessment, J. Thorac. Oncol. 5 (9) (2010) 1315–1316.
[66] F. Amersi, N.M. Hansen, The benefits and limitations of sentinel lymph node biopsy, Curr. Treat. Options Oncol. 7 (2006) 141–151.
[67] M. Moslehi, A. Shanei, S.M.R. Hakimian, et al., 99mTc-phytate lymphoscintigraphy for detection of sentinel node: preliminary results of the first year's clinical experience in Isfahan, Iran, J. Med. Signals Sens. 5 (1) (2015) 69.
[68] C.-C. Ho, Y.-H. Chen, S.-H. Liu, et al., Optimal imaging time for Tc-99m phytate lymphoscintigraphy for sentinel lymph node mapping in patients with breast cancer, Tzu-Chi Med. J. 31 (3) (2019) 163.
[69] C. Tsopelas, R. Sutton, Why certain dyes are useful for localizing the sentinel lymph node, J. Nucl. Med. 43 (10) (2002) 1377–1382.
[70] H. Shankar, P.S. Pagel, D.S. Warner, Potential adverse ultrasound-related biological effects: a critical review, J. Am. Soc. Anesthesiol. 115 (5) (2011) 1109–1124.
[71] S. Cho, M. Kim, J. Ahn, et al., An ultrasensitive and broadband transparent ultrasound transducer for ultrasound and photoacoustic imaging in-vivo, Nat. Commun. 15 (1) (2024) 1444.
[72] C. Qiu, B. Wang, N. Zhang, et al., Transparent ferroelectric crystals with ultrahigh piezoelectricity, Nature 577 (7790) (2020) 350–354.
[73] S. Lu, J. Yang, T. Wei, et al., Single-incision endoscope-assisted breast-conserving surgery and sentinel lymph node biopsy: prospective SINA-BCS cohort study, Br. J. Surg. 110 (9) (2023) 1076–1079.
[74] Z.-H. Wang, T.-R. Gang, S.-S. Wu, et al., Single-port endoscopic-sentinel lymph node biopsy combined with indocyanine green and carbon nanoparticles in breast cancer, Surg. Endosc. 37 (10) (2023) 7591–7599.
[75] Z.H. Wang, X. Qu, C.S. Teng, et al., Preliminary results for treatment of early stage breast cancer with endoscopic subcutaneous mastectomy combined with endoscopic sentinel lymph node biopsy in China, J. Surg. Oncol. 113 (6) (2016) 616–620.

Moongyu Han Dr. Moongyu Han received his Ph.D. degree in Creative IT Engineering at Pohang University of Science and Technology (POSTECH) in Republic of Korea from 2020 to 2024. He is currently undertaking a post-doctoral researcher training course at POSTECH (2024 ~). His research interests include the development of photoacoustic /ultrasound imaging devices, their clinical applications to determine clinical significance, and their commercialization.

Young Joo Lee Young Joo Lee, M.D., MS, is currently serving as a Clinical Assistant Professor in the Division of Breast Surgery, Department of Surgery, at Seoul St. Mary's Hospital, Catholic University of Korea, Seoul, Korea. He completed his premedical and medical education at Hallym University, Chuncheon, Korea, earning his M.D. degree in 2010. He later pursued a Master of Medicine degree at the University of Ulsan, College of Medicine, Seoul, Korea, graduating in 2020, and is presently enrolled in the Ph.D. program at the same institution. His research and clinical interests focus on breast cancer surgery, including advanced surgical techniques and multidisciplinary care.

Junho Ahn Junho Ahn is a Ph.D. candidate in Electrical engineering at Pohang University of Science and Technology (POSTECH) in Republic of Korea. He completed his B.S. in physics at POSTECH in 2017. His research interests include ultrasound and photoacoustic imaging, ultrafast Doppler imaging, and their clinical translation.

Sunghun Nam Sunghun Nam is a Ph.D. candidate in the Department of Electrical Engineering at Pohang University of Science and Technology (POSTECH). He received his B.S. degree in Electrical Engineering from POSTECH in 2022, and currently, his research interests include the development of photoacoustic and ultrasound imaging systems for clinical applications.

Minseong Kim Minseong Kim is a Ph.D. candidate in Convergence IT Engineering at Pohang University of Science and Technology (POSTECH). He completed his B.S. and received his M.S. in Mechanical Engineering at POSTECH (2018–2024). His current research interests focus on the development of photoacoustic and ultrasound imaging systems and their clinical applications.

Jeongwoo Park Dr. Jeongwoo Park earned his Ph.D. degree from the School of Interdisciplinary Bioscience and Bioengineering at Pohang University of Science and Technology (POSTECH), Republic of Korea. He is currently an Assistant Professor in the Department of Biomedical Convergence Science and Technology at Kyungpook National University, Daegu, Korea. His research interests are advanced ultrasound transducers, ultrasound imaging, ultrasound therapy, photoacoustic imaging, and multimodal imaging for both preclinical and clinical applications.

Joongho Ahn Joongho Ahn received his B.S degree in Electronics Engineering at Kyungpook National University, South Korea in 2016, and did his Ph.D. degree in Convergence IT Engineering at Pohang University of Science and Technology (POSTECH), South Korea in 2022. He worked as a Postdoctoral Research Associate and is currently a Research Assistant Professor of the Department of Electrical Engineering at POSTECH. He holds an additional position as a senior researcher in Opticho, which is a spin-off startup from POSTECH. His research interests include the development of biomedical imaging systems with optics, ultrasonics, and/or photoacoustics, and their clinical translation and commercialization.

Hanyoung Ryu Han Young Ryu received the Ph. D. degree in physics from the Chungnam National University, Daejeon, Korea, in 2006. Since 2006, he was worked as a Senior Researcher in the Division of Physical Metrology, Korea Research Institute of Standards and Science, Daejeon, Korea. Since 2011, he is working as a Principle Research Engineer in the WonTech Company. His current research interests include fiber laser, mode-locked fiber laser, nonlinear fiber optics, optical fiber comb generator. Dr. Ryu is a Member of the Optical Society of Korea, Korean Physical Society.

Youngseok Seo Young-Seok Seo is currently the Director of R&D center of WON TECH Co., Ltd. Daejeon, Korea, working on medical laser devices research and development. He obtained a joint Ph.D. degree in physics from Chungnam National University and Korea Atomic Energy Research Institute (KAERI), in February 2003. From March 1999 to September 2003, he had been with Quantum Optics Laboratories of the KAERI, working on high-power laser delivery system by adaptive optics (AO) technologies such as wavefront sensing, aberration compensation, and closed-loop control of AO systems. In October 2003, he joined Laser Power Photonics Group of the Institute of Laser Engineering (ILE) at Osaka University, Osaka, Japan where he has been engaged in optical fiber communication research. Among his research interests are fiber amplifiers, fiber lasers, and new laser materials. In October 2006, he returned to KAERI and established High energy laser facility of KAERI.

Byullee Park Dr. Byullee Park is an assistant professor in the Department of Biophysics at the Institute of Quantum Biophysics, Sungkyunkwan University (SKKU). He earned his Ph.D. at Pohang University of Science and Technology (POSTECH). His research focuses on developing advanced imaging systems, including photoacoustic, optical, and acoustic modalities, as well as innovative sonoepigenetic platforms. By integrating these technologies, Dr. Park aims to advance medical science and improve our understanding of complex biological processes.

Dooreh Kim Dooreh Kim graduated from Yonsei University College of Medicine and obtained a Master's degree in Medicine in 2024 from Yonsei Graduate School. She is currently pursuing a Ph.D. program in Medicine at the Catholic University of Korea. Her research is centered on advancing breast cancer treatment, with a particular emphasis on integrating cutting-edge medical technologies.

Chulhong Kim Chulhong Kim earned his Ph.D. degree and did postdoctoral training at Washington University in St. Louis, Missouri. He currently holds the Young Distinguished Professorship and Mueunjae Chair Professorship, and is a professor of Convergence IT Engineering, Electrical Engineering, Mechanical Engineering, Medical Science and Engineering, and Medical Device Innovation Center at Pohang University of Science and Technology in the Republic of Korea. He is a Fellow of IEEE, SPIE, OPTICA, and AIMBE. His research interests include the development of clinical photoacoustic/ultrasound imaging scanner, fast optical-resolution photoacoustic microscopy based on a 2-axis water-proof MEMS scanner, AI-based biomedical image enhancement, etc.